

AD-A115 205

WASHINGTON UNIV SEATTLE

F/G 8/11

CRUSTAL STRUCTURE NEAR THE ICELAND RESEARCH DRILLING PROJECT 80--ETC(U)

1980 W H THOMSON, J D GARMANY, B T LEWIS

N00014-78-C-0389

UNCLASSIFIED UW-CONTRIB-0000

NL

1 of 1
AD-A
1982



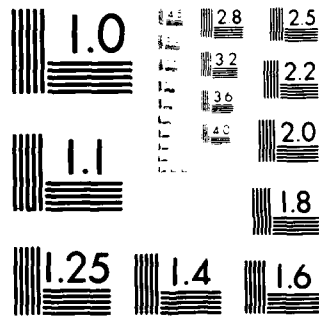
END

DATE

FILED

10782

DTIC



MICROCOPY RESOLUTION TEST CHART
NATIONAL BUREAU OF STANDARDS-1963-A

*In press in Journal of Geophysical
Research*
(2)

CRUSTAL STRUCTURE
NEAR THE
ICELAND RESEARCH DRILLING PROJECT BOREHOLE
FROM A SEISMIC REFRACTION SURVEY

N00014-78-C-0309

William H. Thomson*
Jan D. Garmany
Brian T. R. Lewis
Geophysics Program and Department of Oceanography
University of Washington
Seattle, WA 98195

AD A115205

DTIC FILE COPY

*Now at Shell Oil Company
New Orleans, Louisiana

UW Contribution No. 0000

DISTRIBUTION STATEMENT A
Approved for public release;
Distribution Unlimited

DTIC
SELECTED
JUN 7 1982
S H D

82 05 25 156

ABSTRACT

A seismic refraction survey was conducted at Reydarfjörður, Iceland as part of the Iceland Research Drilling Project in July, 1978. An array of 15 seismometers was used to measure apparent velocities from 25 explosions along a 23 km refraction line. The experiment yielded data used to determine the P and S-wave velocity structures beneath the drill site and to obtain bounds on the depth to seismic "layer 3". The observed apparent velocities vary continuously as a function of range with a marked increase in velocity at a range of 16 km. This corresponds to an observed cross-over in the travel time data. The measurement of apparent velocities has yielded data of the form $X(p)$, the distance to a measured ray parameter, and $\tau(p)$, the delay time.

Joint inversion of the $X(p)$ and $\tau(p)$ data has been performed by linear programming. Layers of constant slowness gradient are used as the basis for the inversion process. Estimates of error in the data are used to produce extremal bounds on the family of earth models that satisfy the data.

The resulting envelope of P-wave velocity models indicates a continuous variation of velocity with depth. Two regions of high velocity gradient are observed, one near the surface and the other at depths between 2.6 and 3.9 km associated with "layer 3" in Iceland. These results suggest that modeling of Iceland's upper crust with a few thick homogeneous constant velocity layers is an inadequate representation of the velocity structure.

DTIC
COPY
INSPECTED
2

Accession For	
NTIS GRA&I	<input checked="" type="checkbox"/>
DTIC TAB	<input type="checkbox"/>
Unannounced	<input type="checkbox"/>
Justification	
By	
Distribution/	
Availability Codes	
Dist	Avail and/or Special
A	

INTRODUCTION

The primary objective of the seismic experiment at Reydarfjörður was to determine the P and S-wave velocity structure underlying the Iceland Research Drilling Project site. The refraction survey was laid out to allow determination of a velocity model for the stratigraphy sampled by the 1.9 km deep borehole and to allow comparison of the results of field seismic methods with those of lab analysis of rock physical properties. In situ measurements of seismic velocities provide us with a more integrated velocity vs. depth model, averaged over local heterogeneities as opposed to the discrete sampling done in laboratory analyses of rock velocities.

The refraction experiment was designed to produce a bounded estimate of the depth to "layer 3" velocities in the vicinity of the drill site. Palmason (1963, 1970) suggested that "layer 3" velocities may be within 3 km of the surface in northeastern Iceland and possibly shallower beneath tertiary volcanic centers. The close proximity of Thingmuli, a Tertiary volcano approximately 5 km west of the drill site, suggests that this seismic layer may be close to the surface along the refraction profile. This possibility was investigated by generating and recording waves refracted by this layer. A line with shot to receiver separation up to 23 km was used to sample "layer 3" velocities. Array recording of closely spaced shots was used to provide resolution for measuring velocity gradients as a function of depth.

Finally, this paper investigates the appropriateness of homogeneous layered interpretations of refraction data. The use of thick planar layers of constant velocity for the purpose of modeling travel time data has been prevalent for many years in seismic refraction interpretation although there are many reasons to believe that velocity varies continually with depth. A

thick layered crustal model generally represents an overconstrained solution to the inverse problem and is an artifact of the modeling technique and sparsity of data. Therefore, the inversion applied to the data here allows the determination of a velocity function that varies continuously as a function of depth.

Experiment Description

The refraction survey at Reydarfjörður utilized a densely-spaced array of seismometers and an unreversed line of shots. The use of a fixed array minimizes error in the measurement of apparent velocities because individual station corrections can be easily determined. Measurement of the apparent velocities across an array is equivalent to the direct measurement of p , the ray parameter. The resolving power of the array is dependent on the array length, number of sensors and frequency of seismic energy propagating across it. A shorter array decreases resolution in measured p while a longer array smooths out the variability of the measured ray parameters. In refraction surveys where a closely spaced array is not used, $p = dT/dX$ (the slope of the time-distance curve) is often approximated by fitting a smooth curve to sparse T, X data. This interpolation approach may introduce artifacts into the interpretation. Therefore, we have used the array measurements of ray parameter for the determination of velocity structure.

The refraction survey was conducted on a line west to east with shots ranging from 1.5 km to 20 km east of the drill site (Figure 1). A 15-channel digital recording array was used in two configurations to yield T, X data and phase velocities. In the first configuration, the seismometers were placed in a closely spaced array centered about the drill site for a total spread of 2.4 km. Eleven shots were fired between 1.5 km and 8 km east of the drill site. These explosions were detonated in shallow water to enhance acoustic coupling.

Following these shots, nine of the seismometers were moved farther west of the drill site to create an array of 6 km spread. These were located on the flank of Thingmuli volcano at considerably higher elevation than the other stations. This move enabled recording of refracted rays whose bottoming points were close to the drill site to sample the velocities beneath. In this part of the experiment, shots were located in the fjord from 7 km to 20 km east of the drilling project in 10-20 meters of water.

Joint Inversion of $\tau(p)$ and $X(p)$ data

The analysis of the Reydarfjörður data is based on the measurements of apparent velocity with the array. The data have been reduced to estimates of $X(p)$, the distance to a given ray parameter and $\tau(p)$, the delay time function. Given an infinite number of $X(p)$, $T(x)$, or $\tau(p)$ data containing no observational errors, it would be possible (in the absence of low velocity zones) to find a unique earth model satisfying the data exactly. With data sampled at discrete points it is only possible to place bounds on a family of solutions. The existence of observational errors in the data further increases the range of possible models that fit the data. Numerous inversion methods have been devised to treat bounds on either $X(p)$ data (e.g., McMechan and Wiggins, 1972) or $\tau(p)$ data (e.g., Bessonova et al., 1974, 1976) and to produce estimates on the range of earth models that satisfy the constraints of the data. However, because bounds on the $X(p)$ and $\tau(p)$ data represent independent information, it is desirable to utilize them together as simultaneous constraints in the inversion process.

The inversion applied here utilizes a scheme for the joint treatment of $X(p)$ and $\tau(p)$ data as formulated by Orcutt (1980) following the linear programming approach of Garmany et al. (1979). In this approach a stack of

layers of constant gradient of slowness is used to approximate a continuous velocity vs. depth variation. The functions $X(p)$ and $\tau(p)$ are represented as linear functions of $z(p)$ (Dorman, 1979) and the seismic inversion solved using linear programming. This produces extremal bounds on the depth to a given value of p subject to the constraints of the data and the physical "realizability" of the solution (Garmany et al., 1979).

Determination of the $X(p)$ and $\tau(p)$ data was accomplished by the construction of record section plots of all seismograms recorded for a single shot (e.g., Figure 2). The regression line $T = \tau + pX$ was fit to the first arrival picks (T, X) using the least squares criterion. The time intercept of the line is our estimate of tau and the slope of the line is our estimate of p over the array interval. The value of X was chosen to be equal to the mean shot-to-receiver distance to produce the $X(p)$ estimates. Some secondary arrivals were inferred from the record sections to provide information on the extent of the triplication.

Because the instruments were used as a closely-spaced array for only half of the shots, an alternate method was used for determination of $X(p)$ for the configuration where the receivers were more widely spaced. A second order polynomial was fitted to the (T, X) data using the least squares criterion. The ray parameter, p , was computed for the mean of X and compared to p computed by linear regression. The values of p computed by polynomial regression did not vary significantly from those computed by linear regression so the latter values were used in the modeling and inversion processes.

To facilitate the placement of bounds on the $X(p)$ data, confidence limits for p were computed at the 95% probability level assuming a normal distribution of the (T, X) data about the line $T = \tau + pX$. These limits were used

together with the scatter in the $X(p)$ data to infer upper and lower bounds for the envelope of all possible $X(p)$ values as shown in Figure 3. Values of $\tau(p)$ were determined similarly where τ is the time intercept of a regression line fitted to the (T, X) data. The values of $\tau(p)$ for the secondary arrivals was inferred from record section plots of the seismograms and these points were added to the $\tau(p)$ data to represent the retrograde branches of the travel time data. The scatter in all of the $\tau(p)$ data provided a final constraint on the placement of bounds on the $\tau(p)$ curve as shown in Figure 4.

Compressional Wave Velocity Profile

The extremal slowness-depth model for the compressional waves was obtained by the joint inversion of the $X(p)$ and $\tau(p)$ data bounds contained in Figures 3 and 4. These bounds on depth to a given slowness are plotted in Figure 5. Two zones of high slowness gradient appear in the model, one in the top .5 km of crust and the other between depths of 2.6 and 3.9 km. The former can be attributed to surface weathering and porosity variation. Because porosity decreases with depth due to greater overburden pressure, the observed velocities increase as a function of depth. The second zone of high slowness gradient can be identified as the "layer 3" boundary. Although this boundary has been commonly modeled as an abrupt increase in velocities, it appears that a transitional region of increase occurs over nearly 1 km in depth. This contention is based on the small X -extent of triplication in the travel time curves and the lack of obvious reflections and secondary arrivals from this region.

The structure determined here does not contain the features of homogeneous layers often modeled in refraction surveys. Instead, slowness decreases continually as a function of depth as evidenced by decreasing values of ray parameter with increasing distance. This results from the use of analysis that

requires a continual velocity depth variation and not from the technique of modeling a finite number of layers with discrete values of velocity.

Shear Wave Velocity Profile

Because of the sparsity of good S-wave data, it has been necessary to fit a simple layered solution to the S-wave data. The travel times of specific phases of the emergent S-waves were measured and a standard "layer cake" inversion was performed. This has produced a three-layered model of constant velocity layers for the S-wave structure (Figure 6).

Knowledge of V_s and V_p are aids in determining the physical properties of rocks at depth. The values of V_s determined here agree fairly well with those of Pálmason (1971), although the "layer 3" velocities here are slightly higher. Because of the uncertainty associated with the measurement of V_s and the continual variation of V_p , the computed values of Poisson's ratio exhibit a range of values, from .26 to .30. Pálmason's values for layers 1, 2 and 3 are all approximately .27 with standard deviations of .02 due to a much greater number of samples.

Two-Dimensional Structure

The refraction experiment at Reydarfjörður yielded information that can only be used to estimate a single dimension of velocity variation. However, one feature of the data suggests the possibility of a dip of "layer 3" in this area. The apparent velocities measured for waves refracted by this layer are consistently higher than values reported elsewhere in Iceland. The apparent velocities reported here vary from 6.6 to 7.1 km/sec, increasing with range while Pálmason (1971) found velocities of 6.35 km/sec with a standard deviation of .21 km/sec based on 72 independent measurements. The higher velocities observed at Reydarfjörður could be attributed to an eastward dipping interface beneath the west end of the refraction line. Only a moderate degree of dip

(roughly 3 degrees) is necessary to explain the increase in apparent velocities. This supports Pálmason's view that "layer 3" in Iceland may be nearer the surface beneath Thingmuli and other major Tertiary volcanic centers.

The approach taken in this analysis has assumed only one dimension of velocity variation. Although there is some evidence of a more complex structure, the lack of a reversed refraction profile precludes a two-dimensional modeling. The presence of dipping or nonplanar velocity structure may slightly alter the depths to a given velocity but the observed gradients will be the same.

A Shallow Low Velocity Zone

A casual inspection of Figure 7 shows that the travel times obtained from the velocity depth model derived from apparent velocities across the array do not fit the time-distance data particularly well, and, in addition, there is a rapid attenuation of the first prograde branch beyond 10 km distance. This attenuation does not seem to be correlated with the experimental procedure (movement of the seismometers, for instance) and it has a continuous behavior so that one would presume that it is real. It is conceivable that a form of lateral heterogeneity might be responsible for these observations, but the gross features can also be modeled with a laterally homogeneous structure with a shallow and rather extreme velocity inversion.

The reflectivity method was used to calculate synthetic seismograms (Fig. 8). The first model used had a gradient zone that lay within the extremal bounds down to 2 km (the depth of the borehole) where various low velocity zones were inserted. The only model that gave a reasonably good fit to the observed first arrivals was one with an abrupt and extreme inversion (down to 4 km/s). However, such a sharp change in structure gave rise to prominent reflections at short distances. The original data were examined for such reflections, and

it appears likely that they are present (Fig. 9). These four T_1, X_1 pairs were used to construct a Clairaut envelope (Bessonva et al., 1974) from which a portion of the delay time curve for these reflections was inferred. The bounds to this reflector were 1.65 to 2.51 km depth. It is interesting to note that a reflectivity run with the low velocity zone at 1.75 km depth yielded a much sharper attenuation of first arrivals at 10 km, and actually looked more like the data, but this placement is not consistent with laboratory velocity measurements (Christensen and Wilkens, this volume).

Although the 1.9 km core does not show any obvious lithologic change that could be identified with this reflector or velocity inversion in the lower kilometer, the other drilling results show that there is a sequence of highly impermeable layers beginning at about 1.2 km depth (Fig. 10). It is conceivable that high pore pressure due to water trapped under these layers could lead to an in situ velocity reduction which would not be observed in laboratory velocity measurements.

N. Christensen (personal communication) feels that pore pressure is an unlikely means of obtaining the lowered velocities, and has suggested that thermal effects are more significant. It is always possible to argue that refraction experiments yield lateral averages of structures, and that the lid of the low velocity zone just happens to be out of reach of the drill hole. Only a few hundred meters of relief in the lid surface would be required to do this. The particular velocity in the low velocity zone of 4 km/s is conjectural, since it is possible to trade off thickness versus velocity, even, to some extent, with synthetic seismogram modeling.

DISCUSSION AND CONCLUSIONS

In the initial design of this experiment it was planned to deploy an array of seismometers which could be used to obtain phase velocities directly and these in turn used to invert for velocity as a function of depth. The rationale was that this method is insensitive to time perturbations under individual shots, which would not feasibly be determined.

As the analysis of the time-distance data has shown non-uniqueness due to low velocity zones is a real problem and a low velocity zone cannot be excluded by the T-P data (Figure 4). However, a comparison of the synthetic seismograms with the data in Figure 7, in particular the cusp region from 12 to 20 km, shows that the low velocity model still is not an ideal fit to the data. If we allow for the possibility of inhomogeneities causing time delays under the shot points, especially the two shots at 13 and 15 km, then the low velocity interpretation might be less attractive.

With these reservations the following can be concluded from this study.

(1) Modeling of the upper crust in Iceland with a few homogeneous constant velocity layers is inadequate. Velocity varies continuously with depth apart from the possibility of an abrupt decrease near 2 km depth. Velocity increases near the surface may be attributed in part to a decrease in porosity with depth.

(2) There are two regions of high positive velocity gradient in the upper crust, one near the surface and the other at depth between 2.6 and 3.9 km. The near surface gradient is probably due to weathering and fracturing. The deeper region represents "layer 3" and probably is associated with a metamorphic transition.

(3) The contention that "layer 3" in Iceland is locally shallow beneath Tertiary volcanic centers appears valid. However, the drill hole did not reach sufficient depth to sample it.

- McMechan, G.A. and R.A. Wiggins (1972) Depth limits in body wave inversions, *Geophys. J. R. Astr. Soc.*, 28, 459-473.
- Orcutt, J.A. (1980) Joint linear, extremal inversion of seismic kinematic data, *J. Geophys. Res.*, 85, 2649-2660.
- Palmason, G. (1960) Seismic refraction investigation of the basalt lavas in eastern Iceland, *Jökull* (Reykjavik), 13, 40-60.
- _____ (1971) Crustal structure of Iceland from explosion seismology, Rit. 40, Reykjavik: *Society Scientific Iceland*, 187 pp.
- Walker, G.P.L. (1959) Geology of the Reydarjördur area, eastern Iceland, *Quart. J. Geol. Soc. London*, 114, 367-391.

FIGURE CAPTIONS

- Figure 1. Map of refraction configuration in vicinity of Reydarfjörður.
- Figure 2. Record section of shot point 8. All seismograms (unfiltered) recorded for this shot at distance 8.3 km from the array center.
- Figure 3. Envelope of P-wave $X(p)$ data. The solid lines represent smoothed bounds applied to the $X(p)$ data and used as constraints in the inversion for velocity structure.
- Figure 4. Envelope of P-wave $\tau(p)$ data. The solid lines represent smoothed bounds used as constraints on the inversion.
- Figure 5. Bounds on depth found by the joint inversion of $X(p)$ and $\tau(p)$ data (dots). The solid lines represent the inversion of the $X(p)$ bounds alone. The dashed line represents the model used for determining the first arrival time curves plotted in Figure 6.
- Figure 6. Record section of shots recorded by stations 4, 5 and 6. A continuous velocity model was used to determine the P-wave travel time curve. A layered model was used to determine the S-wave travel times.
- Figure 7. Resulting one-dimensional velocity models. The S-wave model is a simple layered solution. Pálmason's S velocities are also shown (vertical bars). The P-wave model places extremal bounds on the range of possible depths to a given velocity.
- Figure 8. Three sets of synthetic seismograms derived from structures with low velocity zones. The phase with velocity about 4 km/s seen at all distances is a numerical artifact.
- a) Model 1. An extreme inversion (down to 4 km/s) at 2 km depth. Prograde branch is too strong at distances greater than 10 km.

b) Model 2. Inversion at 1.5 km. Prograde energy is now too small at 10 km. This depth was inconsistent with linear programming estimate of depth to reflector (> 1.6 km).

c) Model 3. Inversion at 1.75 km. Prograde energy closer to observations, caustic due to layer 2-3 boundary is better placed.

Figure 9. The four seismograms recorded nearest to the shot showing probable reflections.

Figure 10. Permeability log from the IRDP hole. Note the presence of highly impermeable layers between 1.2 and 1.7 km depth. (From Johnson and Rummel, this volume.)

13°50'W
65°05'N

64°55'N

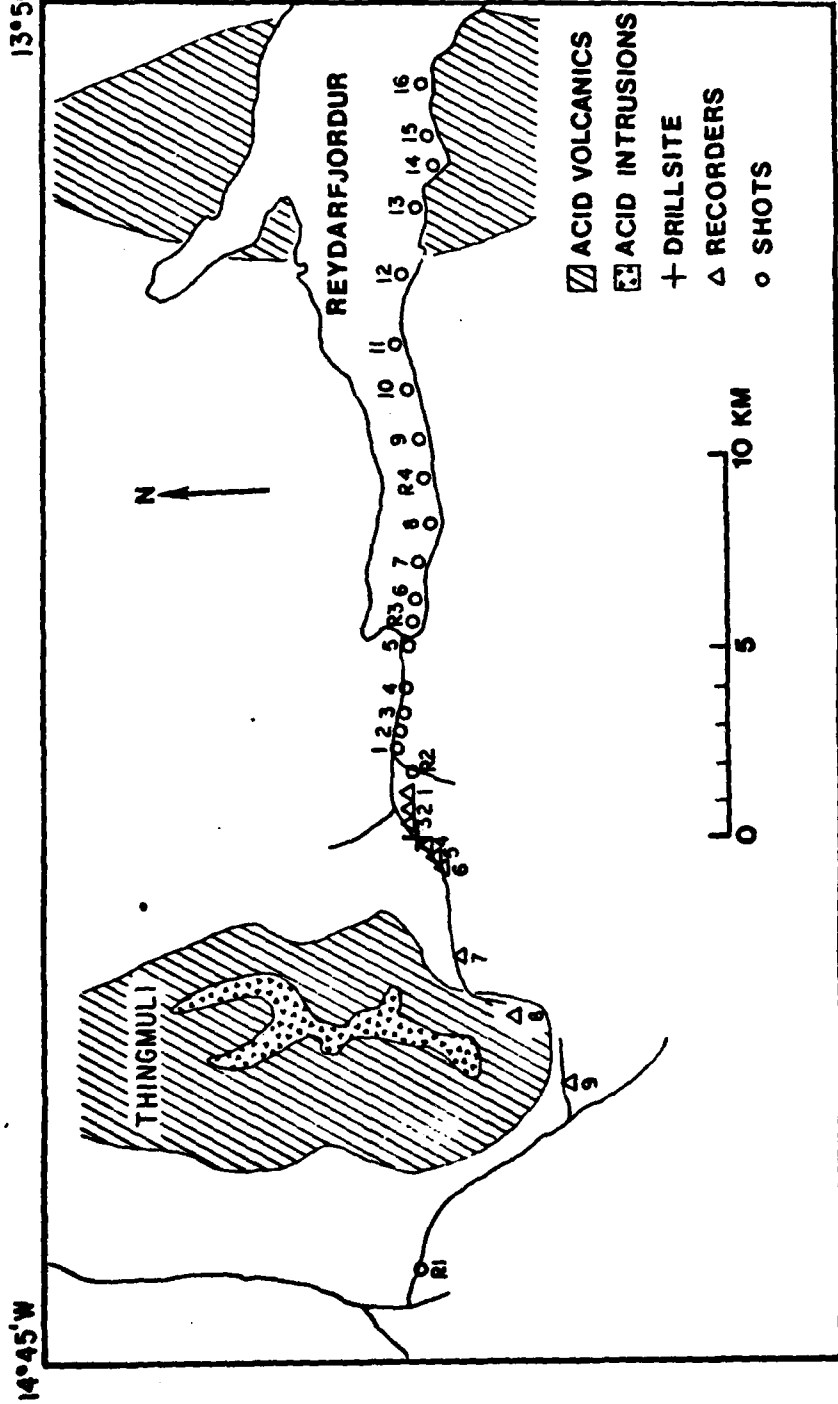


Fig. 1

TIME (SEC)

DISTANCE (KM)

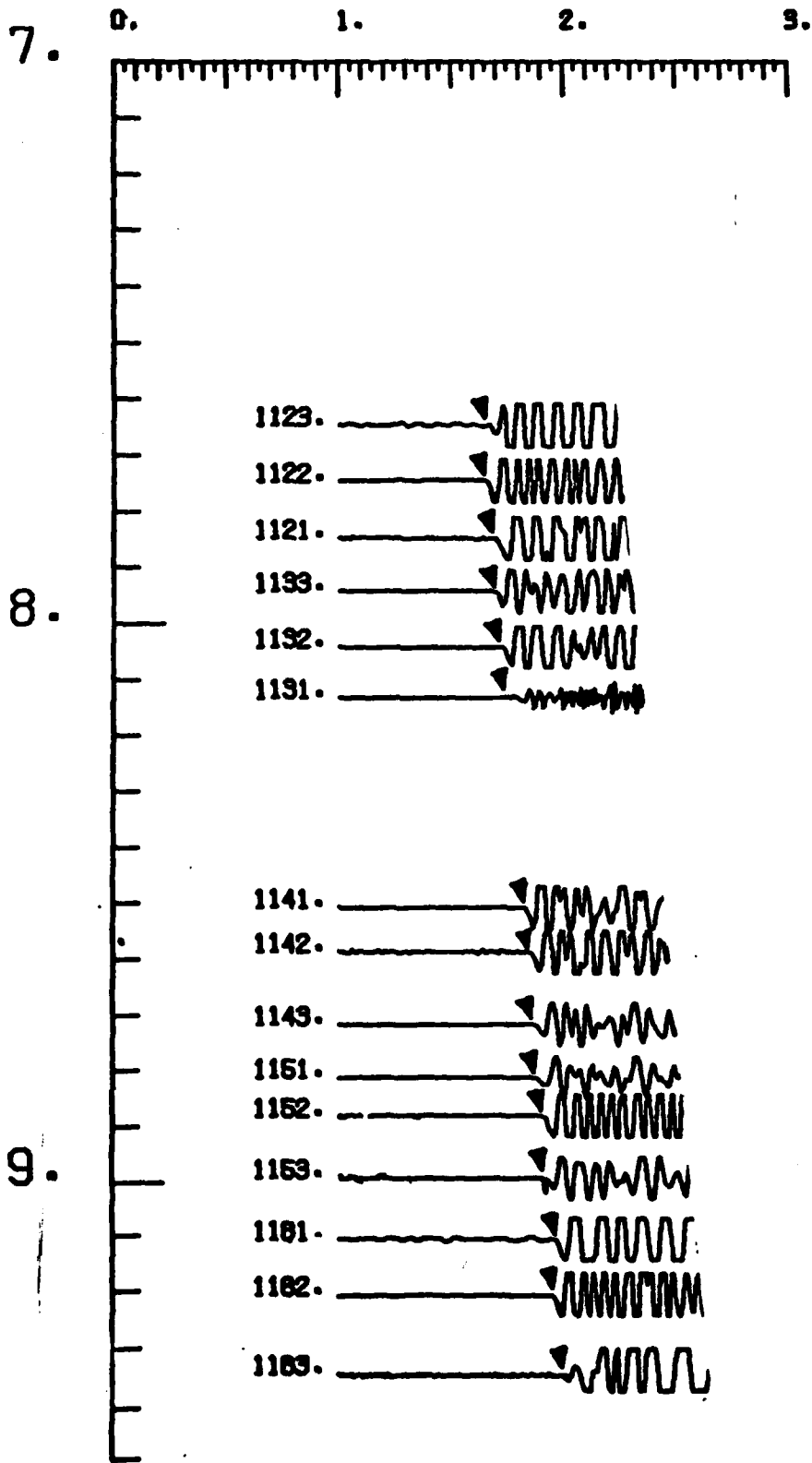
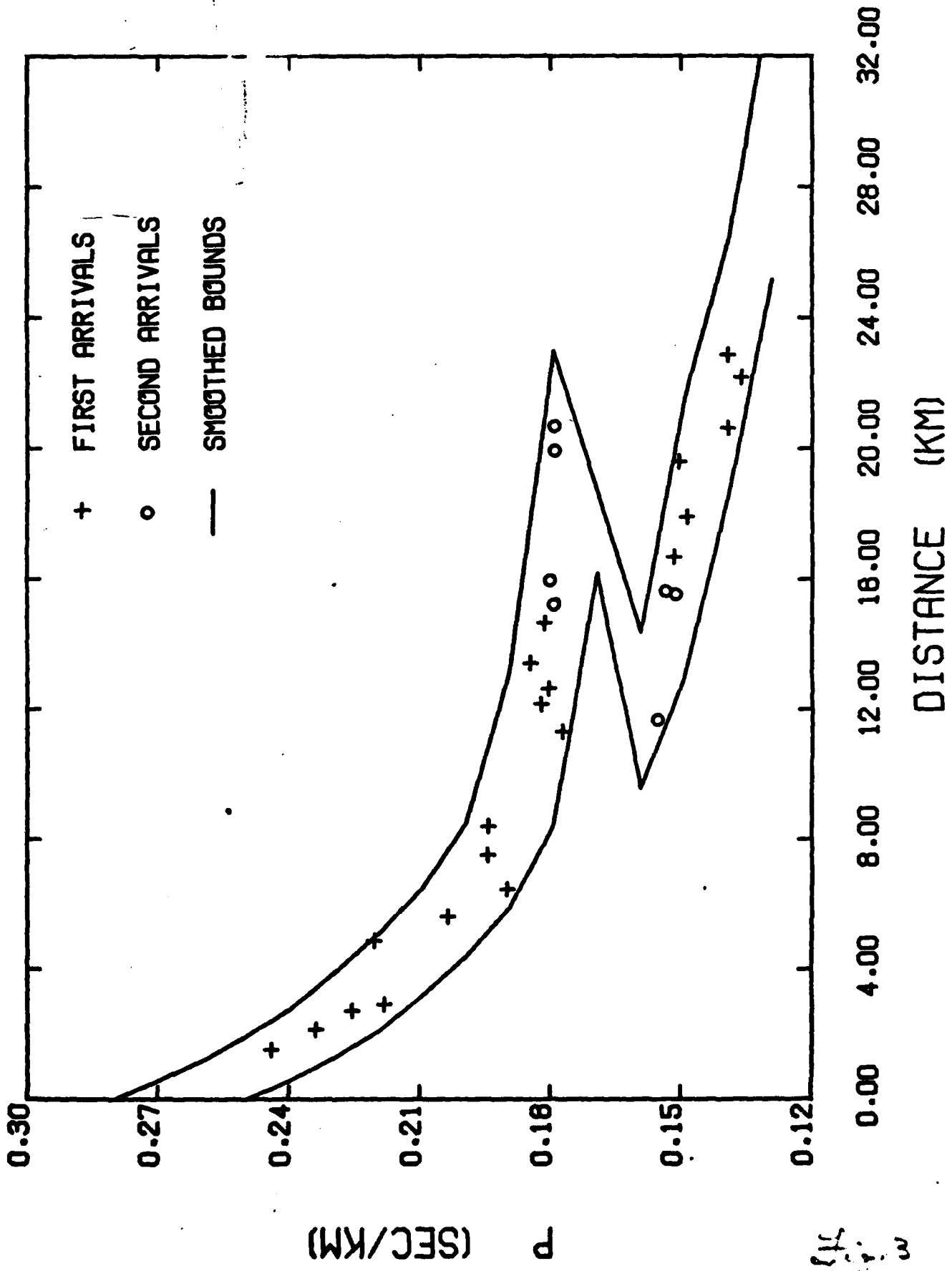


Fig. 2



111
 54
 3

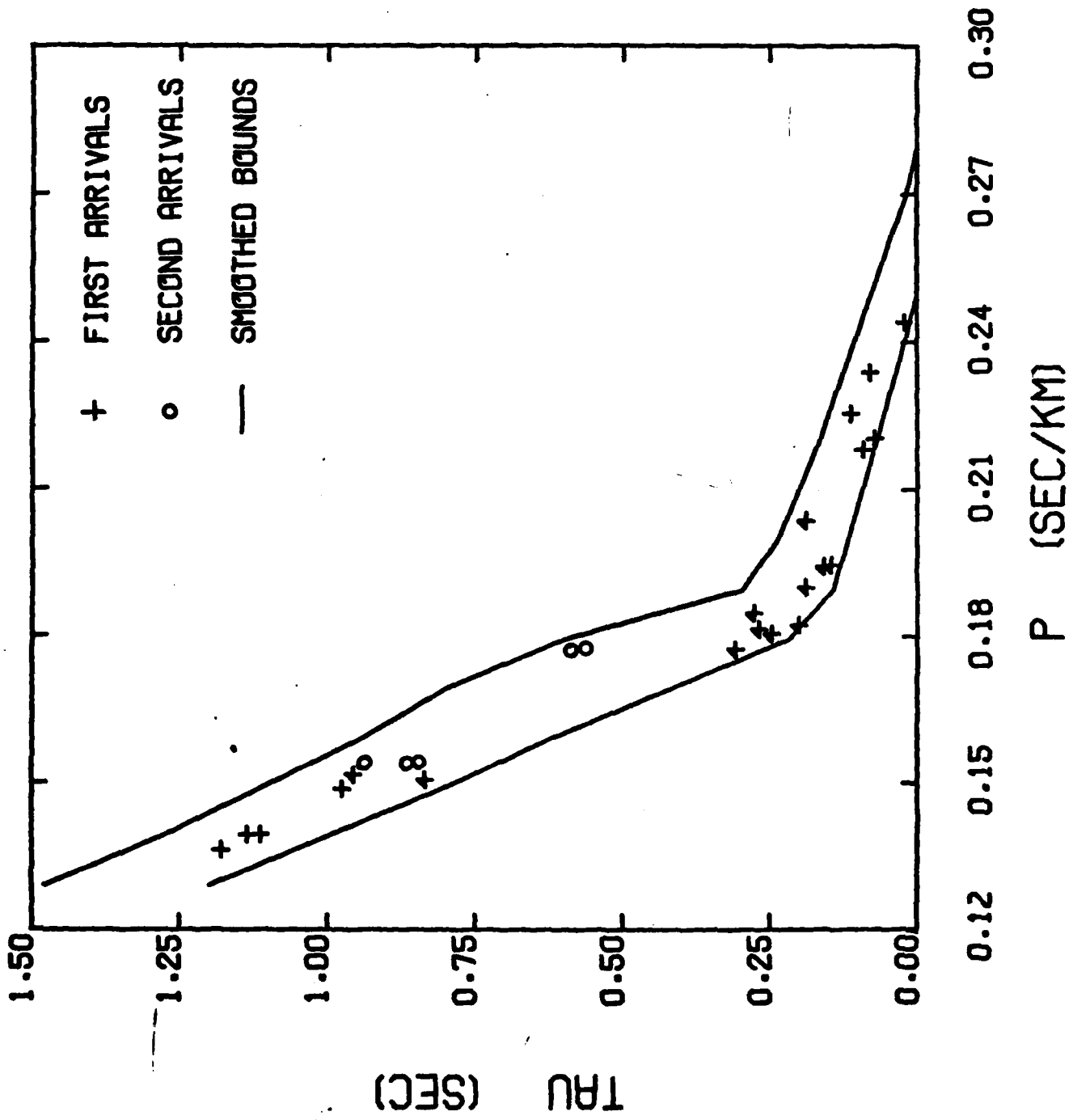


Fig. 4

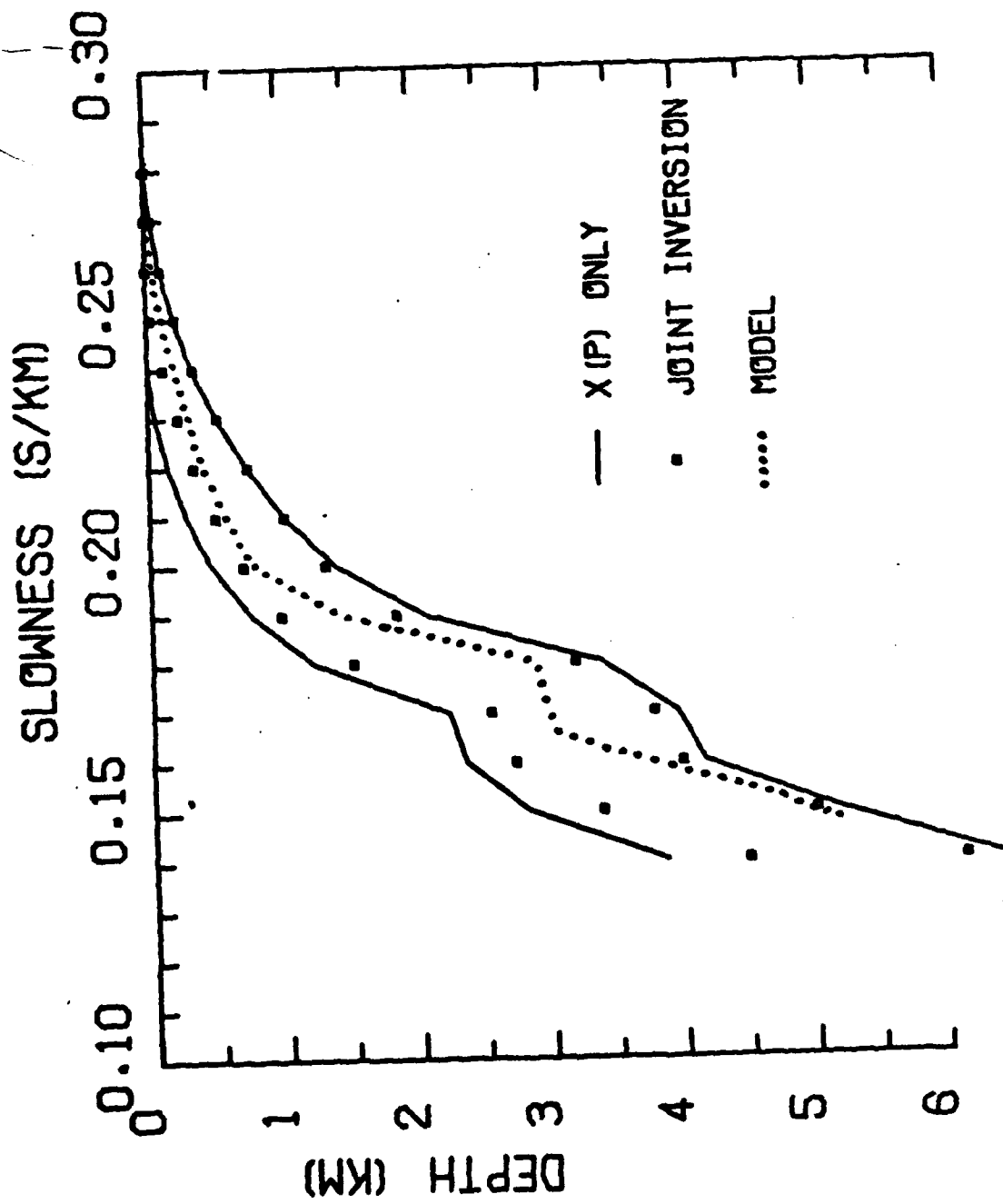


Fig. 5

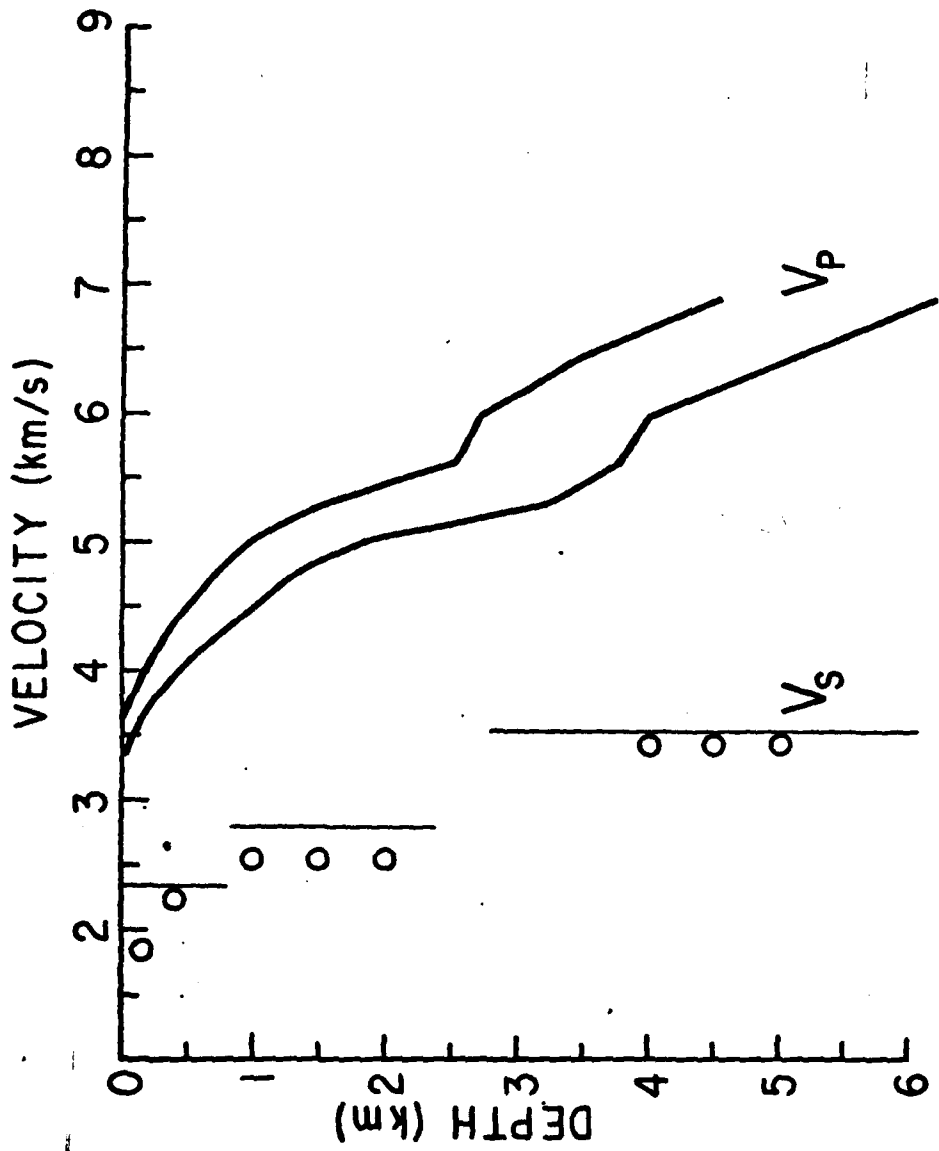


Fig. 6

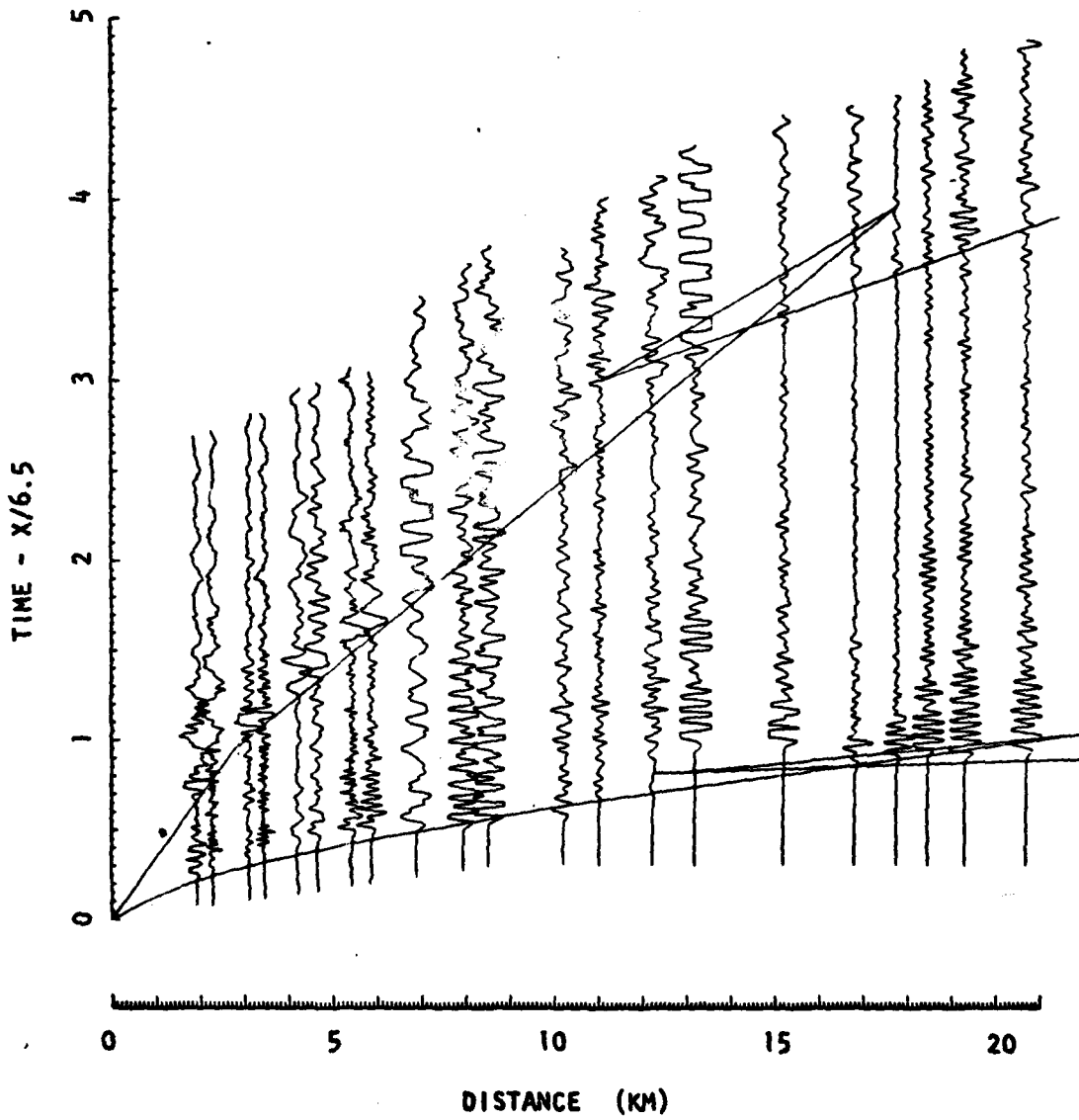


Fig. 7

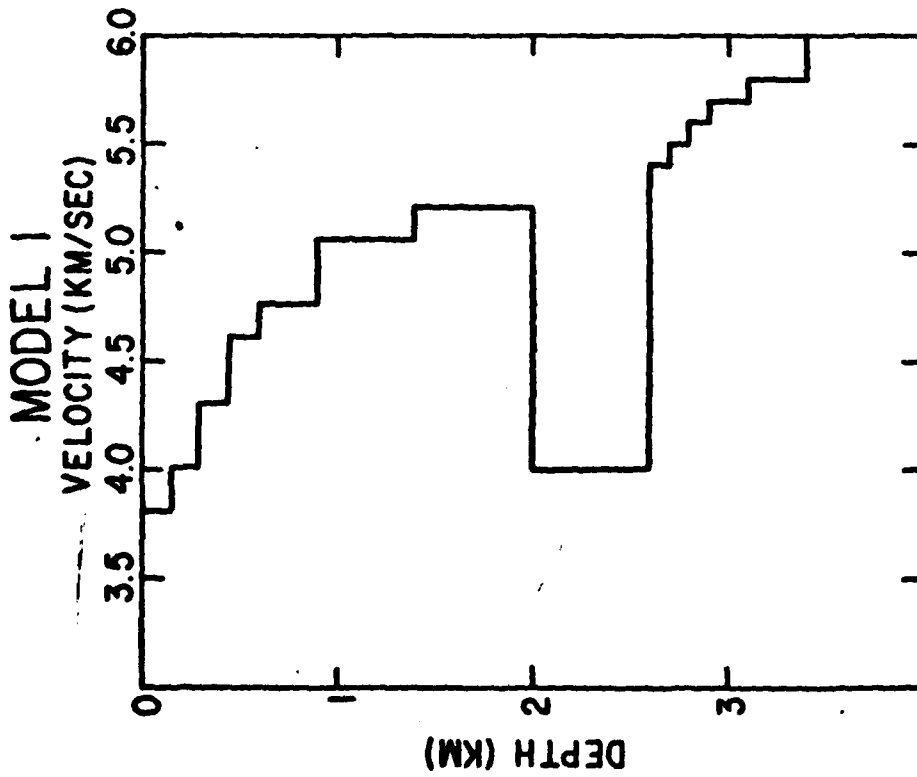
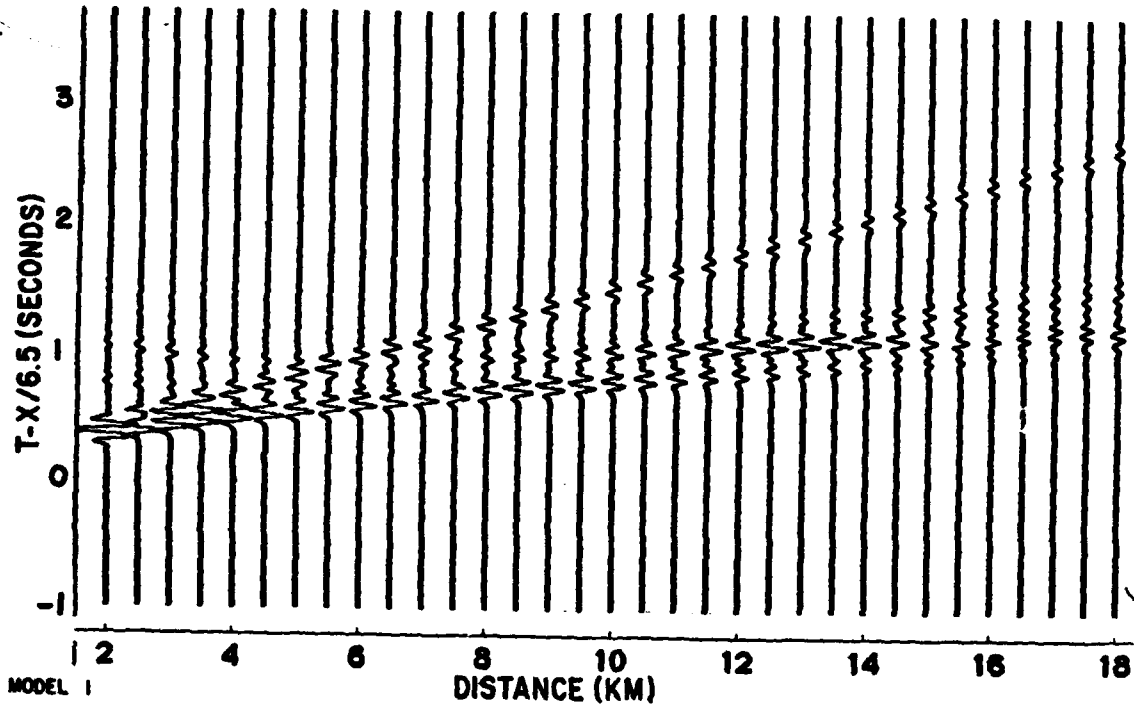


Fig. 8

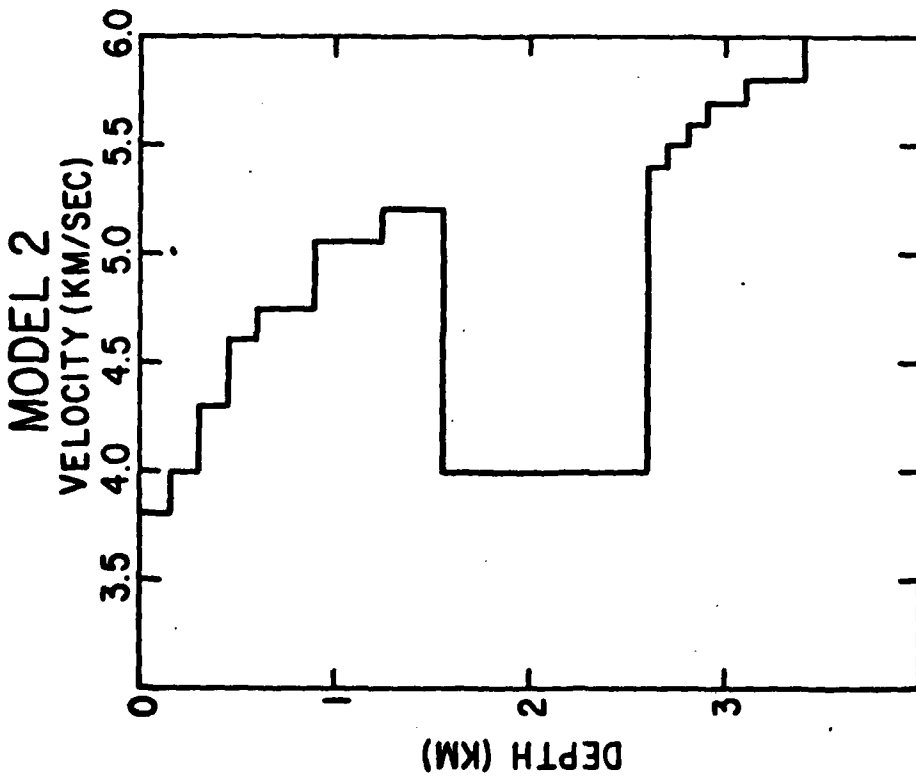
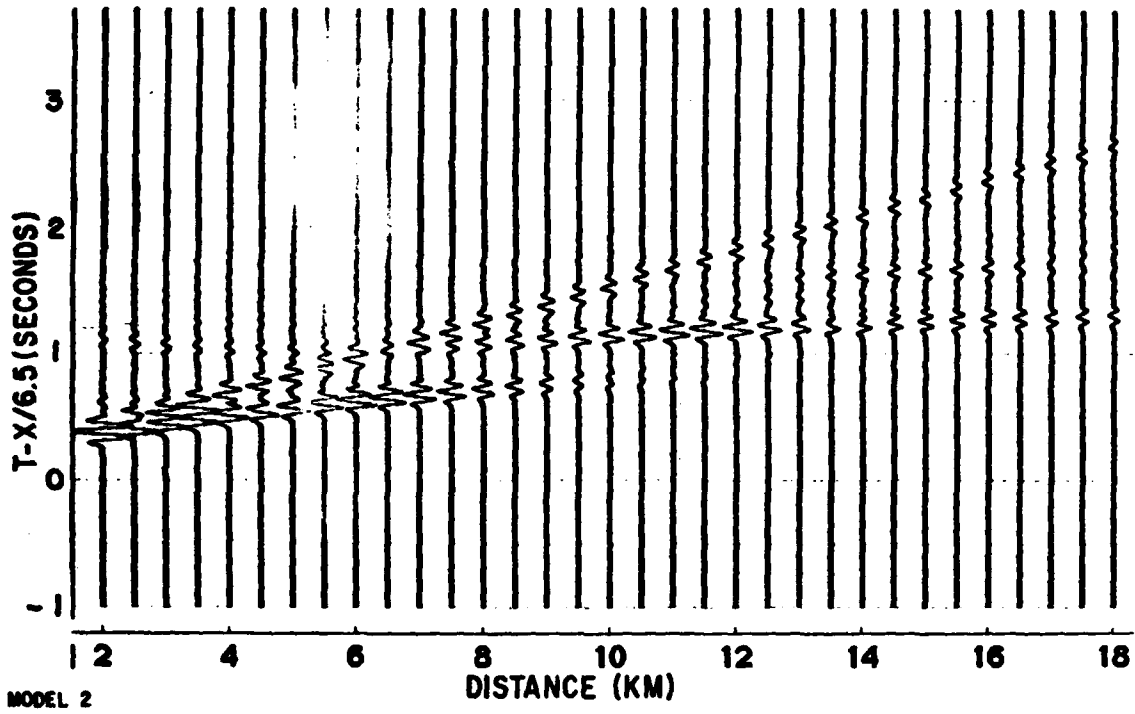


Fig. 9

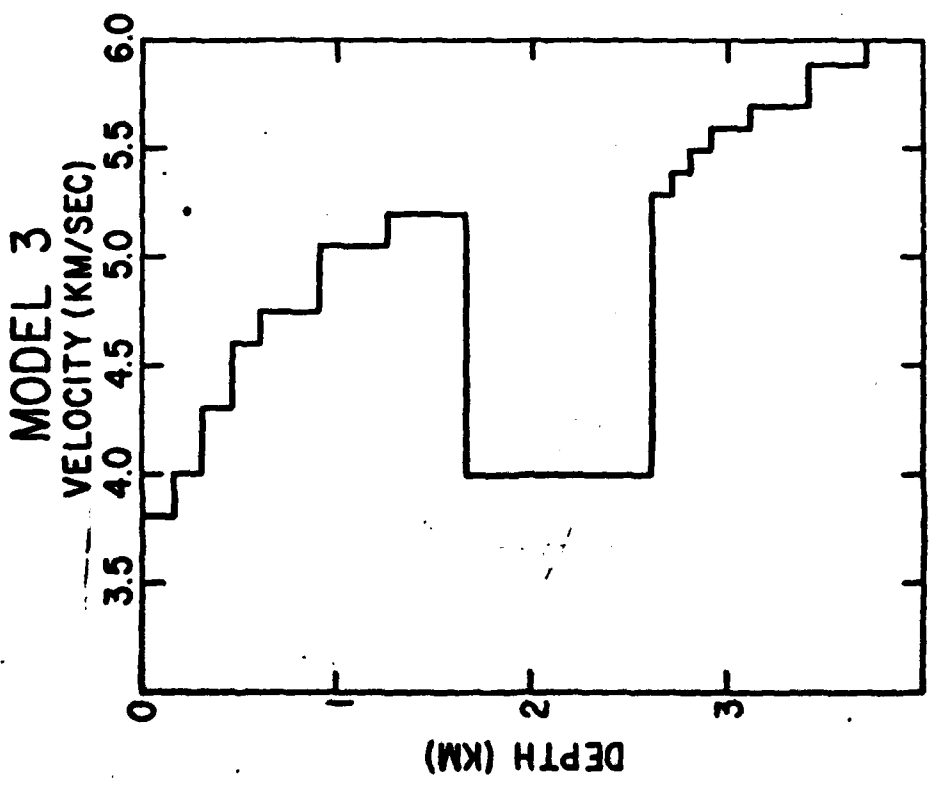
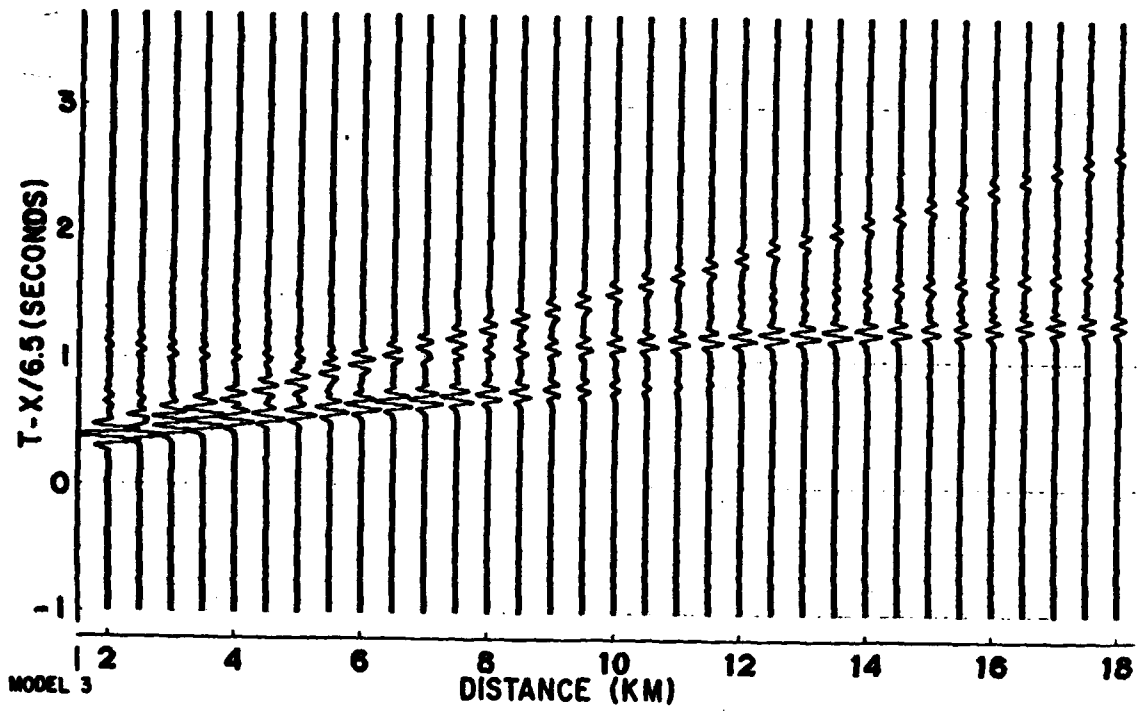
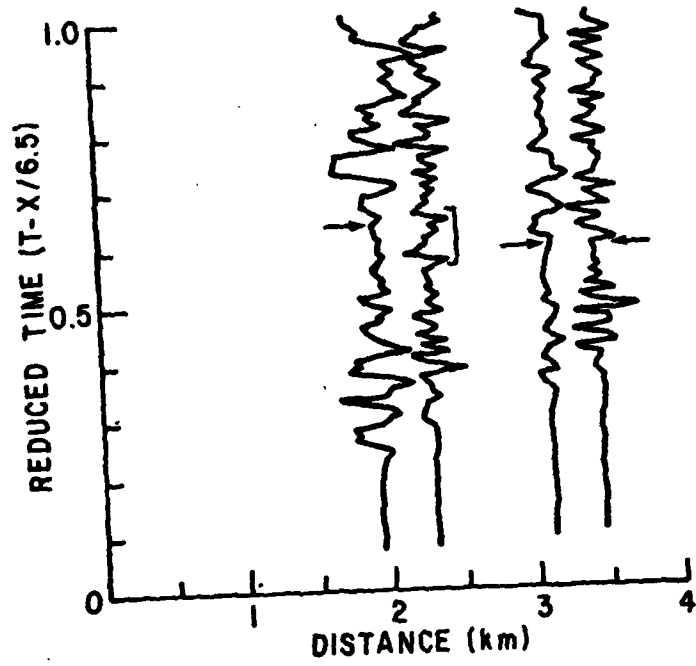


Fig. 10



11
11

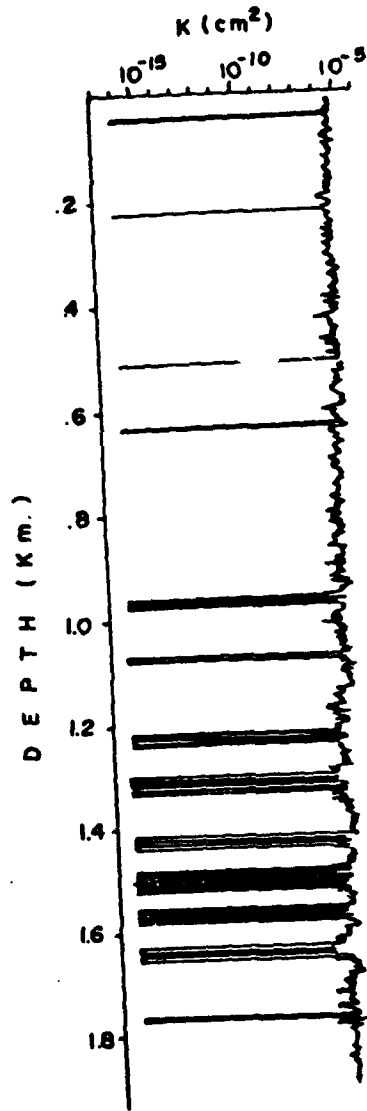


Fig. 12

FIL
7